

# Potentiality of graphene as a base material for impact ionization avalanche transit time diode in high-frequency applications

Mamata Rani Swain<sup>1</sup>, Pravash Ranjan Tripathy<sup>2</sup>

<sup>1</sup>Department of Electronics and Communication Engineering, Biju Patnaik University of Technology, Rourkela, Odisha, India

<sup>2</sup>Department of Electronics and Communication Engineering, Gandhi Engineering College, Bhubaneswar, Odisha, India

---

## Article Info

### Article history:

Received Jun 1, 2023

Revised Oct 30, 2024

Accepted Jan 25, 2024

---

### Keywords:

Efficiency

Graphene

Impact ionization avalanche

transit time

RF power

Self-consistent drift diffusion

---

## ABSTRACT

In this paper, the microwave application potential of graphene is studied using a double-drift-region (DDR) impact ionization avalanche transit time (IMPATT) diode. The simulation of this diode is carried out for the very first time at several different atmospheric window frequencies. Because graphene has unique and special properties, it could be used to make electronic gadgets for the next generation. The device is simulated at a variety of millimeter and sub-millimeter wave frequencies using a model called self-consistent drift diffusion (SCDD), which was developed by the author based on current continuity, Poisson's equation and space charge equation. When compared to traditional IMPATT devices such as Si, GaAs, InP and GaP, the results demonstrate superior performance in terms of efficiency, and RF power across a wide range of operating conditions. Again, the behavior of noise in graphene IMPATT is studied, and it is found that it makes less noise than Si and GaAs IMPATT. The simulation results open up new avenues for IMPATT diode manufacture and design.

This is an open access article under the [CC BY-SA](#) license.



---

## Corresponding Author:

Mamata Rani Swain

Department of Electronics and Communication Engineering, Biju Patnaik University of Technology

Rourkela, Odisha, India

Email: swain.mamata201@gmail.com

---

## 1. INTRODUCTION

Impact avalanche transit time (IMPATT) diodes made from different types of semiconductors have become one of the most important areas of study in the last 30 years because they are so powerful and efficient. Researchers are paying more attention to the microwave (1-30 GHz), millimeter-wave (30-300 GHz), and sub-millimeter-wave (300-500 GHz) frequency bands. This is because people want faster, wider, and more accurate wireless connections. More attention is being paid by the semiconductor business to new materials and devices that could make devices work better or add new functions to them. A recent study by [1], [2] has shown that materials based on graphene are used in electrolyte-gated transistors and biomedical instruments. Geim tested graphene as one of the thinnest and strongest material (in the nm range) in the universe whose charge carrier exhibits giant intrinsic mobility [3]. Ghivela and Sengupta [4] suggested that graphene is becoming the next-generation electronic material due to it is single atomic layer that is zero-band gap and excellent electronic properties like high electrical conductivity, high electron mobility, and tenability. Ghivela and Sengupta [5] developed a graphene-silicon carbide (SiC) double drift region (DDR) IMPATT diode due to its practical and attractive electronic features. Zhao *et al.* [6] reviewed the significance of “graphene-on-surface” structures and investigated the properties and distinct applications including optoelectronics, surface catalysis, anti-friction and super lubricity, and coatings and composites. Nayana and Vimala [7] made a model to test the transfer properties of a single-layer and double-layer graphene field

effect transistor and showed that graphene has an ambipolar property. Marhoon and Qasem [8] proposed a graphene-tuned single/array rectangular microstrip patch antenna (MPA) with inset feed that works in different frequency bands. Al-Mudhafar and Jawad [9] suggested adding graphene nanoantenna arrays as nanoelectrodes to the silver nanowire-based photomixer to improve conductivity. Acharyya [10] modelled static, high-frequency, and noise performance of a parallel connected GNR-based IMPATT structure for power-combining mm-wave and terahertz frequencies. Ghivela and Sengupta [11] studied graphene-based IMPATT diodes with transverse magnetic fields. Computer technique analyses graphene-based DDR IMPATT diode space charge research. High junction temperatures provide extra space charge in the avalanche zone. GIMPATT's decreased space charge resistance and stabilizes DC-to-RF conversion efficiency. GIMPATT's decreased avalanche-to-drift voltage ratio further boosts conversion efficiency [12]. Ghivela [13] demonstrated a graphene-based heat sink for a double-drift region IMPATT device.

However, research on microwave, mm-wave, and terahertz (THz) transit time devices has been limited. Insufficient evidence suggested that graphene could be utilised in microwave, millimeter-wave, and THz applications, which was one of the reasons why it was not utilised more. This paves the way for further investigation into graphene devices applicable to microwave, millimeter-wave, and THz technologies. However, the potential of this approach is limited by the noise caused by the random nature of impact ionization in the active space charge area. IMPATT diode can be used for various purposes as a radio generator. So, it is very important to understand how noise is made and how it behaves when the signal is small if you want to build and run IMPATT diodes in the best way possible [14]-[16].

This study examines the suitability of graphene as the fundamental material for DDR IMPATT diodes, which are designed to operate at frequencies inside the millimeter-wave and sub-millimeter-wave window frequencies of 94, 140, 220, 300, and 500 GHz are investigated for prospective microwave applications. The small-signal characteristics of graphene DDR IMPATT devices were compared to conventional IMPATT devices made of silicon (Si), gallium arsenide (GaAs), gallium phosphide (GaP), and indium phosphide (InP). Again, graphene DDR IMPATTs devices outperformed Si and GaAs substrates in noise performance.

## 2. PROCESS OF DESIGN AND MATERIAL PARAMETERS

Figure 1 depicts the one-dimensional (1-D) DDR-based IMPATT ( $n^+$ - $n$ - $p$ - $p^+$ ) diode studied in this simulation. The IMPATT device works because the frequency of the charge carriers depends on how long it takes for them to move the transit time ( $\tau_T$ ). Sze and Ryder [17] first set up the IMPATT for a certain design frequency ( $f_d$ ) using the empirical formula  $w_{n,p}=0.37 v_{sn, sp}/f_d$  where  $v_{sn}$ ,  $v_{sp}$  are the electron and hole drift speeds at saturation, and  $w_n$ ,  $w_p$  are the widths of the n-side and p-side depletion areas. As operating frequency rises, depletion layer lowers. Charge density rises as depletion width decreases. Electric field increases with operation frequency because it is proportional to charge density integral. The depletion layer electric field and carrier current profiles are needed to measure the IMPATT diode's DC characteristics. The models do not account for the widths of the  $n^+$  and  $p^+$  zones, despite the presence of significant doping in these regions. The doping concentrations of the n- and p- layers are initially chosen to be on the order of  $10^{23} \text{ m}^{-3}$ , taking into consideration the design frequencies. Table 1 depicts graphene's structure and doping parameters at millimeter-wave and sub-millimeter-wave frequencies.

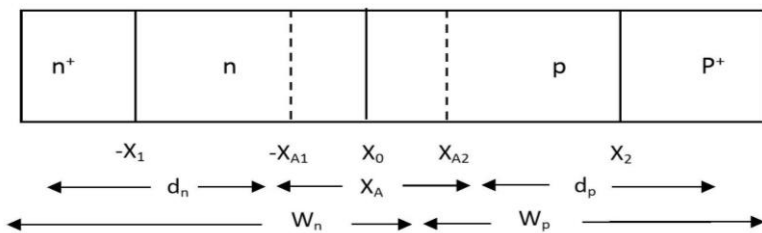


Figure 1. One dimensional (1-D) model of DDR IMPATT of graphene ( $n^+$ - $n$ - $P$ - $P^+$ )

From newly published reports, the field-dependent saturated drift velocities ( $v_{sn}$ ,  $v_{sp}$ ), field-dependent ionization rates ( $\alpha_n$ ,  $\alpha_p$ ), field dependent mobilities ( $\mu_n$ ,  $\mu_p$ ), and other material parameters such as width-dependent band gap ( $E_g$ ), permittivity ( $\epsilon$ ), effective masses ( $m_n^*$ ,  $m_p^*$ ), intrinsic carrier concentration ( $n_i$ ), the effective density of states of the conduction band and valence band ( $N_c$ ,  $N_v$ ), diffusion coefficients ( $D_n$ ,  $D_p$ ) of graphene at 300k are added to the simulation programme [18]-[25].

Table 1. Design parameters of graphene

Si No	f <sub>d</sub> (GHz)	W <sub>n</sub> (μm)	W <sub>p</sub> (μm)	N <sub>D</sub> (×10 <sup>23</sup> m <sup>-3</sup> )	N <sub>A</sub> (×10 <sup>23</sup> m <sup>-3</sup> )	D <sub>i</sub> (μm)
1	94	2.755	2.716	0.034	0.033	35
2	140	1.85	1.84	0.063	0.059	25
3	220	1.18	1.17	0.1024	0.0921	20
4	300	0.863	0.862	0.1423	0.1401	15
5	500	0.518	0.517	0.27	0.2643	10

### 3. METHOD

The author has made computer programs that combine static, dynamic, and noise analysis in a step-by-step way to calculate the IMPATT diode's dc, small signal, and noise behavior under different working and structural conditions. The details of how IMPATT devices are simulated for DC, small signals, and avalanche noise are given. The proposed technique exhibits characteristics of simplicity, efficiency, precision, and numerical stability due to its adherence to the boundary conditions, which involve initiating the computation from a predetermined peak field value at the metallurgical junction.

#### 3.1. Procedure

To examine the total RF performance of a DDR IMPATT diode, it is necessary to conduct a DC simulation, followed by small-signal simulation, and noise simulation. For the simulation process, the structural and doping parameters, design frequency, all material parameters, and bias current density are entered as inputs.

##### 3.1.1. DC simulation

The study of the IMPATT diode in the direct current (DC) regime involves the simultaneous solution of various device equations. These equations encompass the carrier continuity equation, the space charge equation, and Poisson's equation. The numerical solution of the Poisson in (1) and the carrier continuity (2) was performed concurrently for the double-drift structure of the IMPATT device as shown in Figure 1, with due consideration given to the boundary conditions at the edges of the depletion layer [26]. In the context of the DDR paradigm, specifically with regard to a singular dimension, the equation representing poisson's equation can be expressed as (1):

$$\frac{dE(x)}{dx} = \frac{q}{\epsilon} [N_D - N_A + p(x) - n(x)] \quad (1)$$

E(x) represents the electric field profile, q is electron charge, N<sub>D</sub> and N<sub>A</sub> represent concentrations of donor and acceptor, n(x) and p(x) represent electron and hole concentrations at position x in the depletion layer, and ε represents semiconductor permittivity. The electron and hole continuity equations are (2):

$$\frac{dn}{dt} = \frac{1}{q} \frac{dJ_n}{dx} + g \text{ and } \frac{dp}{dt} = -\frac{1}{q} \frac{dJ_p}{dx} + g \quad (2)$$

Where J<sub>n</sub> and J<sub>p</sub> are the electron current density and hole current density at any point x, respectively, and g is the rate at which carriers are made due to impact ionization.  $g = \alpha_n v_{ns} n + \alpha_p v_{ps} p$ ; α<sub>n</sub> and α<sub>p</sub> are the electron and hole ionization rate. The calculation for the breakdown voltage is as (3):

$$V_B = \int_0^W E(x) dx \quad (3)$$

The drift voltage as V<sub>D</sub>=V<sub>B</sub>-V<sub>A</sub> then the dc to RF conversion efficiency [27] is:

$$\eta(\%) = \frac{2mV_D}{\pi V_B} \quad (4)$$

m=½, the data from the DC analysis is incorporated in to the small signal analysis below. The parameter values collected from DC simulation are shown in Table 2.

Table 2. DC parameters of graphene

Design frequency (GHz)	E <sub>m</sub> (×10 <sup>7</sup> V/m)	V <sub>B</sub> (V)	V <sub>A</sub> (V)	V <sub>D</sub> /V <sub>B</sub> (%)	χ <sub>A</sub> (nm)	χ <sub>A</sub> /w (%)
94	3.027	50.6	33.0	35.7	2,550	46.70
140	4.80	37.4	25.3	32.35	1,750	47.33
220	6.03	28.0	19.9	29.03	1,180	50.17
300	7.28	22.5	16.08	28.5	951	55.07
500	9.5123	16.5	12.8	22.7	598	57.29

### 3.1.2. Small signal simulation

Iterative simulation is used to solve two second-order differential equations that involved diode resistance ( $Z_R$ ) and reactance for small-signal modeling of the IMPATT diode ( $Z_X$ ). After meeting the boundary criteria, this approach [26] calculates a diode's quality factor ( $Q = -B/G$ ) and negative resistance. Numerically integrating the resistivity ( $R$ ) and reactivity ( $X$ ) profiles over the depletion layer width ( $w$ ) yields the total integrated negative resistance ( $Z_R$ ) and reactance ( $Z_X$ ) of diodes at a given frequency.

$$Z_R = \int_0^w R dx \quad (5)$$

$$Z_X = \int_0^w X dx \quad (6)$$

The impedance is described as (7):

$$Z(x, \omega) = R(x, \omega) + jX(x, \omega) \quad (7)$$

The total impedance is calculated by (8):

$$Z_{\text{Total}} = \int_0^w Z(x, \omega) dx = Z_R + jZ_X \quad (8)$$

The negative conductance and susceptance are calculated as (9) and (10):

$$-G = \frac{-Z_R}{[(Z_R)^2 + (Z_X)^2]} \quad (9)$$

$$B = \frac{Z_X}{[(Z_R)^2 + (Z_X)^2]} \quad (10)$$

Calculating the small signal quality factor ( $Q_p$ ) is done as (11):

$$-Q_p = \frac{B_p}{-G_p} \quad (11)$$

Then the RF power obtained from the IMPATT can be calculated as (12):

$$P_{RF} = (V_{RF})^2 |G_p| \times \frac{A}{2} \quad (12)$$

Where  $V_{RF}$  is the RF voltage.

$$V_{RF} = m \times V_B \quad (13)$$

Where  $m$  equals 50%, the peak magnitude of negative conductance at the peak optimum frequency ( $f_p$ ) is  $|G_p|$  and the junction area of the device is  $A (\pi(D_j/2)^2)$ . Here the device's junction diameter is  $D_j$ .

### 3.1.3. Noise analysis

Device noise is caused by the randomness of the impact ionization process and manifests itself as fluctuations in the electric field and DC. Even if no small signal voltage is applied to the diode, these fluctuations appear in the results as a small signal component to DC value. Therefore, noise generation and its effect on the efficacy of the device is a crucial factor for device performance. The graphene IMPATT diode's noise behavior is analyzed using a simulation technique devised in [14].

The noise-free generation rate  $g$  and the noise generation rate  $\gamma$  are the components of the avalanche generation rate. At space point  $x_0$ , a noise source  $\gamma(x')$  can be conditionally expressed as (14):

$$\gamma(x') = \alpha_n(x')v_n(x')n(x') + \alpha_p(x')v_p(x')P(x') \quad (14)$$

At every point in the depletion layer, a noise electric field  $e(x, x')$  is created by the noise source  $\gamma(x')$ . Therefore, the terminal voltage generated by the noise source  $\gamma(x')$  at  $x_0$  is expressed by (15):

$$v_t(x') = \int_0^w e(x, x') dx \quad (15)$$

This defines the transfer impedance as (16):

$$z_t(x') = \frac{v_t(x')}{dI_c(x')} \quad (16)$$

Where  $dI_c(x') = Aq\gamma(x')d(x')$ , the noise source  $\gamma(x)$  is associated with the current that is generated in the space interval  $dx'$  at  $x'$ . Now the mean square noise voltage per bandwidth  $\frac{\langle v^2 \rangle}{df}$  can be determined using the relation.

$$\langle v^2 \rangle = 2q^2 df A \int |z_t(x)|^2 \gamma(x') dx' \quad (17)$$

From which the noise measure (NM), an indicator of noise-to-power ratio, can be obtained following the definition [15].

$$NM = \frac{A\langle v^2 \rangle / df}{4KT(-Z_R)} \quad (18)$$

### 3.2. Instruments and measurements

The recommended IMPATT diode's direct current (DC) characteristic, small signal, and noise performance are modeled using the MATLAB software. The assessment of performance is carried out within the frequency spectrum encompassing millimeter-wave and sub-millimeter-wave.

## 4. RESULT AND DISCUSSION

### 4.1. DC simulation

Table 2 presents the key parameters of graphene DDR ascertained using direct current (DC) simulation, including breakdown voltage ( $V_B$ ), peak electric field ( $E_m$ ), avalanche zone voltage ( $V_A$ ), drift voltage to breakdown voltage ratio ( $V_D/V_B$ ), avalanche width ( $\chi_A$ ), and avalanche width to total depletion layer width ratio ( $\chi_A/w$ ). Figure 2 illustrates how the breakdown voltage, avalanche voltage, and electric field of graphene IMPATT vary with operating frequency. Figure 2 shows that when operating frequency increases, breakdown voltage ( $V_B$ ) and avalanche zone voltage ( $V_A$ ) decrease, while peak electric field ( $E_m$ ) increases. As the operating frequency increases from 94 GHz to 0.5 THz, the maximum electric field ( $E_m$ ) rises from  $3.02700 \times 10^7$  (V/m) to  $9.5123 \times 10^7$  (V/m). The drift voltage ( $V_D = V_B - V_A$ ) can be calculated from the understanding of breakdown voltage ( $V_B$ ) and the avalanche zone voltage ( $V_A$ ). As shown in Table 2, as the working frequency goes up, the ratio of the device's drift voltage to its breakdown voltage ( $V_D/V_B$ ) goes down. At 94 GHz, the value of  $V_D/V_B$  is 0.3572, and it decreases sharply to 0.2278 at 0.5 THz. According to the semi-quantitative formula for the efficiency of DC-to-RF conversion ( $\eta (\%) = (2m/\pi)(V_D/V_B)$ ) [27], as the operating frequency is increased, the DC-to-RF conversion efficiency of graphene IMPATT diminishes drastically.

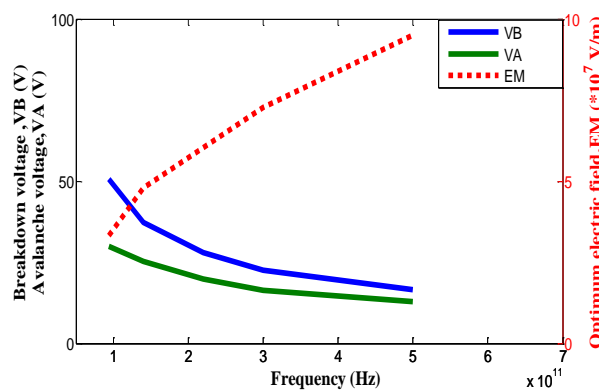


Figure 2. At design frequencies of 94, 140, 220, 300, and 500 GHz, DDR graphene breakdown voltage, avalanche voltage, and ideal electric fields vary

The ratio of avalanche width to total depletion layer width ( $\chi_A/w$ ) in graphene IMPATT significantly increases at higher operating frequencies. Higher  $\chi_A/w$  indicates a wider avalanche zone, leading to higher  $V_A$  and lower drift zone voltage. Lesser  $V_D/V_B$  means lesser conversion efficiency. Thus, the quick growth of the avalanche region at higher operating frequencies in graphene IMPATT diodes causes a dramatic fall in conversion efficiency. In graphene IMPATTs,  $\chi_A/w$  is 46.70 % at 94 GHz and climbs to 57.29 % at 0.5 THz, resulting in a considerable drop in conversion efficiency at 500 GHz.

#### 4.2. Small signal simulation

Table 3 lists the small signal parameters like optimum frequency ( $f_p$ ), peak negative conductance ( $-G_p$ ), corresponding susceptance ( $B_p$ ), quality factor ( $Q_p = -B_p/G_p$ ), efficiency and RF power for  $m=50\%$  at optimized current density. Figure 3 depicts the variations of power  $P_{RF}$  of 94, 140, 220, 300, and 500 GHz with biased current density. At different current densities, the RF power for IMPATT devices increases and remains constant at a particular value. In simulations,  $m$  was changed from 40% to 70% so that the link between  $m$  and RF voltage ( $V_{RF}=m V_B$ ) could be studied. At different current densities, the RF power for IMPATT devices increases and remains constant at a particular value. Figure 4 illustrates the change in power  $P_{RF}$  and efficiency of the DDR graphene IMPATTs with  $V_{RF}$ . Figure 4(a) reveals that the power  $P_{RF}$  initially increases to  $m$  up to 65%, but then decreases  $m$  beyond 60%. The essence of the efficiency versus  $V_{RF}$  is identical about  $m$  in Figure 4(b).

Table 3. Small signal parameters of graphene

Parameter	Value	Value	Value	Value	Value
Design frequency, $f_d$ (GHz)	94	140	220	300	500
Peak frequency, $f_p$ (GHz)	94	145	224	305	504
Efficiency (%)	11.4	10.8	9.50	9.12	7.67
Negative conductance, $G_p (\times 10^7 \text{ Sm}^{-2})$	0.3824	0.9534	1.7552	2.9665	3.6585
Susceptance, $B_p (\times 10^7 \text{ Sm}^{-2})$	0.2141	1.096	3.6926	9.5779	23.225
$Q_p (-B_p/G_p)$	0.56	1.14	2.1.	3.23	6.34
RF power (mW)	1176.88	822.23	540.11	331.36	97.73

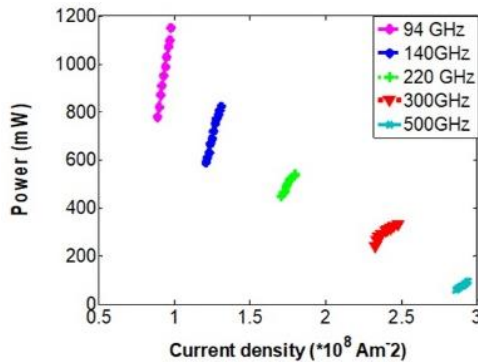


Figure 3. Current density verses RF power DDR graphene IMPATT at 94, 140, 220, 300, and 500 GHz frequency

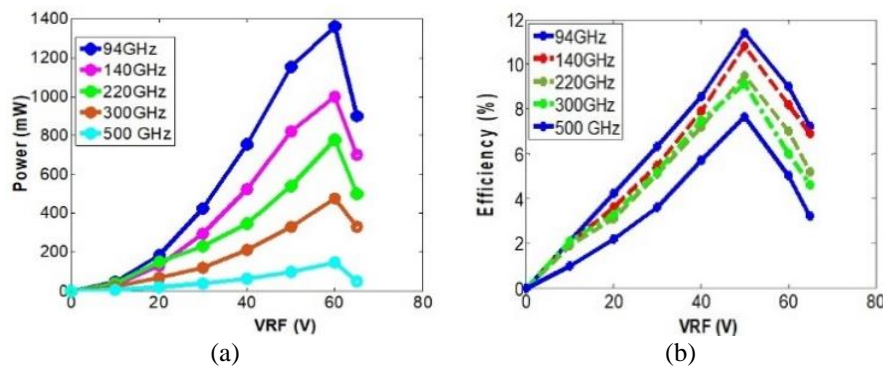


Figure 4. The change in power  $P_{RF}$  and efficiency of the DDR graphene IMPATTs: (a) RF power and (b) efficiency verses RF voltage of DDR graphene IMPATT at 94, 140, 220, 300 and 500 GHz frequency

At design frequencies of 94, 140, 220, 300, 500 GHz, the optimal frequencies ( $f_p$ ) of an IMPATT diode are determined to be 94, 145, 224, 305, 504 GHz. The peak negative conductance and corresponding susceptance values are  $-0.3824 \times 10^7$ ,  $-0.9534 \times 10^7$ ,  $-1.7552 \times 10^7$ ,  $-2.9665 \times 10^7$ ,  $-3.6585 \times 10^7 \text{ Sm}^{-2}$ , and  $0.2141 \times 10^7$ ,  $1.096 \times 10^7$ ,  $3.6926 \times 10^7$ ,  $9.5779 \times 10^7$ ,  $23.225 \times 10^7 \text{ Sm}^{-2}$ , respectively at optimized current density. The conductance versus susceptance (G-B) graph of graphene DDR at 94, 140, 220, 300 and 500 GHz designed frequencies are shown in Figures 5(a) to (e).

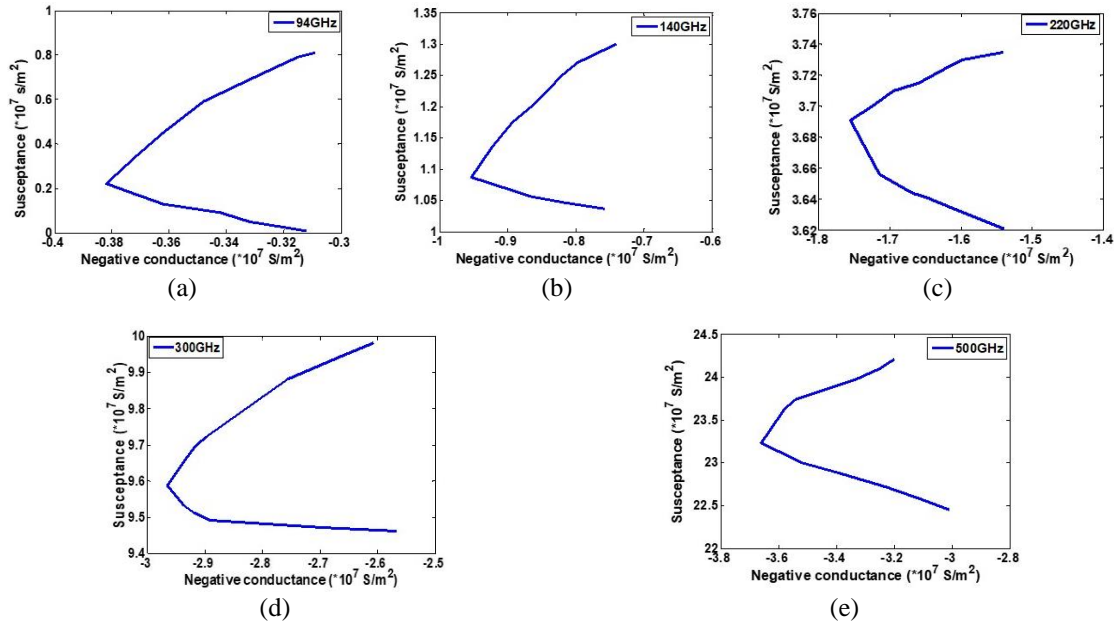


Figure 5. Admittance characteristics of DDR graphene at; (a) 94 GHz, (b) 140 GHz, (c) 220 GHz, (d) 300 GHz, and (e) 500 GHz designed frequency

#### 4.3. Comparison of graphene IMPATT with conventional IMPATT sources based on Si, GaAs, GaP, and InP

Figure 6(a) shows how the working frequency affects the RF power of graphene IMPATT and other conventional sources made of Si, GaAs, InP, and GaP. Figure 6(a) shows that graphene DDR can produce much more RF power than Si (653.35 mW, 378.89 mW, and 297.50 mW) [27] and GaAs (781.37, 227.02, and 177.77 mW) [28] at working frequencies of 94, 140, and 220 GHz, respectively. However, GaP DDR and InP DDR provide marginally more power (1.35 W (InP) and 1.23 W (GaP)) at 94 GHz operating frequency [28], [29]. Nevertheless, graphene IMPATT surpasses its counterparts, namely InP (719.97 and 440.93 mW) [28] and GaP (757.34 and 505.43 mW) [29] at operating frequencies, namely 140 and 220 GHz. At mm-wave frequencies, graphene is better than materials like silicon, gallium arsenide, indium phosphide, and gallium phosphide, which are usually used as base materials. As far as the authors know, there is no experimental study on how well graphene DDR works, so it is impossible to compare the results of experiments. Figure 6(b) compares the efficiency of graphene to that of conventional sources based on Si, GaAs, InP, and GaP, and graphene demonstrates superior efficiency performance. Table 4 compares the parameters of various materials to those of the proposed graphene DDR IMPATT.

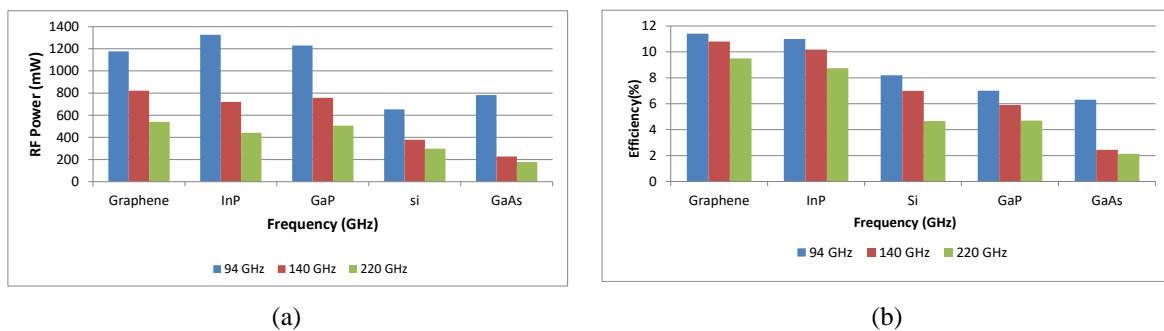


Figure 6. Bar graph of frequency vs: (a) RF power and (b) efficiency of different IMPATT diodes

#### 4.4. Noise properties

Noise is a very important part of IMPATT research, so the noise properties of graphene have been studied and compared to those of IMPATT diodes made of Si and GaAs [16]. Table 5 compares the mean

square noise of graphene, silicon, and gallium arsenide at three different working frequencies: 94, 140, and 220 GHz. From Table 5, we can see that the mean square noise voltage per bandwidth ( $v^2/df$ ) max peaks are at 85, 108, and 145 GHz for working frequencies of 94, 140, and 220 GHz. For Si IMPATT, the highest values of ( $v^2/df$ ) max are 75,100 and 160 GHz and for GaAs, the highest values of ( $v^2/df$ ) max are 60, 110, and 115 GHz. The graphene DDR IMPATT device exhibits the minimum mean square noise voltage across various bandwidths. Figure 7 illustrates the variation in mean square noise voltage per bandwidth of IMPATT diodes as the operating frequency transitions from 94 to 140 GHz and subsequently to 220 GHz.

Table 4. Comparison of different materials' parameters with graphene

Materials	Design frequency, $f_d$ (GHz)	RF power (W)	Efficiency, $\eta$ (%)
Si [27]	94	653.35	8.19
	140	378.89	6.99
	220	297.50	4.66
GaAs [28]	94	781.37	6.31
	140	227.02	2.44
	220	177.77	2.13
InP [28]	94	1326.53	11.00
	140	719.97	10.18
	220	440.93	8.74
GaP [29]	94	1230.00	7.00
	140	757.34	5.90
	220	505.43	4.70
Graphene	94	1176.88	11.4
	140	822.23	10.8
	220	540.11	9.5

Table 5. Noise properties of Graphene concerning Si and GaAs DDR IMPATT diodes

Materials	Frequency at ( $<v^2>/df$ ) <sub>max</sub> (GHz)	( $<v^2>/df$ ) <sub>max</sub> $f_d$ ( $V^2s$ ) (GHz)	( $<v^2>/df$ ) at $f_d$ ( $V^2s$ )	NM at $f_d$ (dB)
Si [16]	75	$1.59 \times 10^{-14}$	94	$1.51 \times 10^{-15}$
	100	$7.7 \times 10^{-15}$	140	$6.51 \times 10^{-16}$
	160	$8.95 \times 10^{-16}$	220	$2.04 \times 10^{-16}$
GaAs [16]	60	$4.52 \times 10^{-14}$	94	$5.54 \times 10^{-16}$
	110	$9.75 \times 10^{-15}$	140	$2.09 \times 10^{-16}$
	155	$3.4 \times 10^{-15}$	220	$5.98 \times 10^{-17}$
Graphene	85	$1.95 \times 10^{-15}$	94	$1.131 \times 10^{-15}$
	108	$7.45 \times 10^{-16}$	140	$3.25 \times 10^{-16}$
	145	$1.17 \times 10^{-16}$	220	$7.38 \times 10^{-17}$

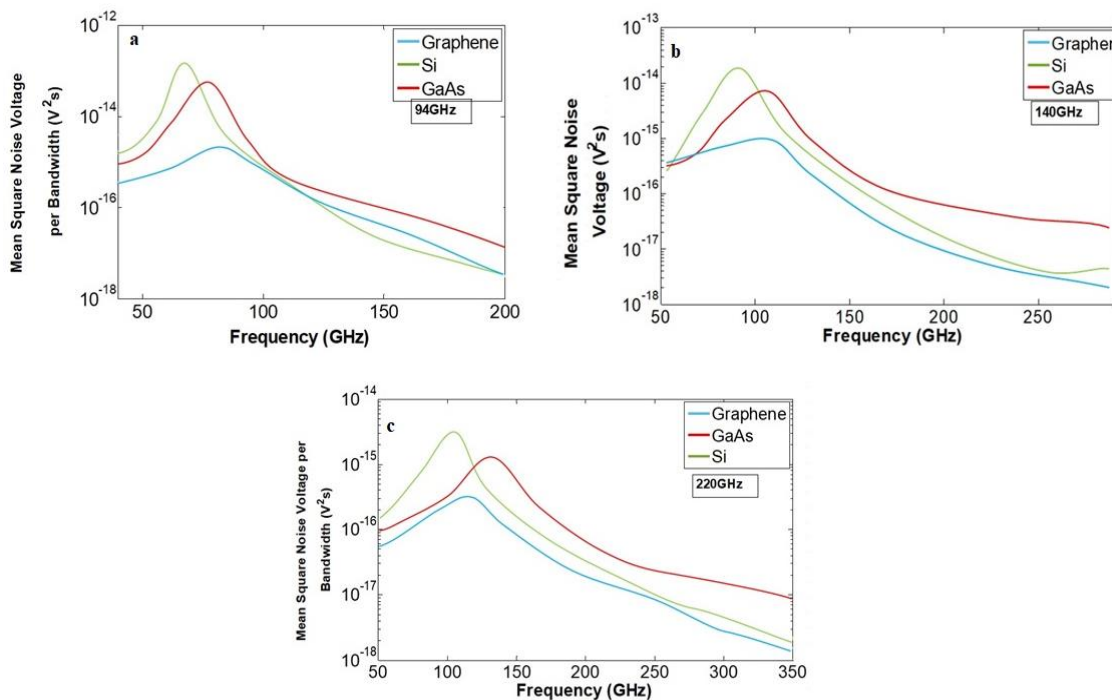


Figure 7. Mean square noise voltage per bandwidth at 94, 140, and 220 GHz

Noise measure (NM), which shows the ratio of noise to power, is a key part of studying noise behavior. Table 5 shows the values of the noise measure that were calculated at the intended frequency. The noise level variation with frequency for graphene, Si, and GaAs is depicted in Figure 8, using distinct operational frequencies of 94, 140, and 220 GHz, correspondingly. Recent studies have demonstrated that graphene exhibits lower levels of noise compared to silicon (Si) and gallium arsenide (GaAs).

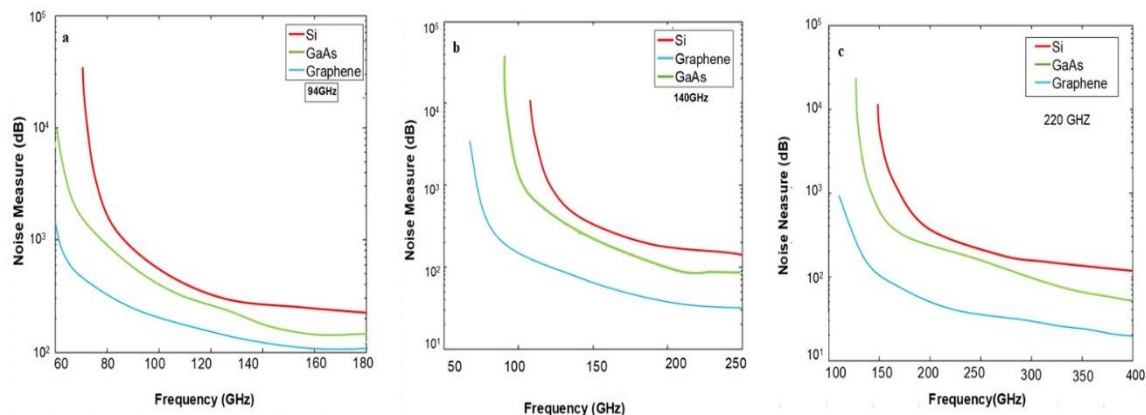


Figure 8. Function of mean square noise voltage per bandwidth vs frequency, 94, 140, and 220 GHz

## 5. CONCLUSION

This research presents an analysis of the performance of graphene-based millimeter-wave and sub-millimeter-wave DDR IMPATTs. Small signal tests and complete DC has been performed on the graphene DDR IMPATTs designed to operate at 94, 140, 220, 300, and 500 GHz window frequencies and the results have been presented in graphs or plots which show that DDR graphene IMPATTs can provide significantly higher RF power and efficiency at millimeter-wave and sub-millimeter-wave window frequencies as compared to Si, GaAs, InP, and GaP. Graphene's DDR structure which possesses microwave-friendly characteristics may be a viable candidate for high-frequency communication system applications. This research aims to elucidate the impact of noise on the D band. Hence, the performance of the IMPATT diode can be improved by carefully choosing the most suitable operating frequency.

## REFERENCES

- [1] S. Vasilijević, R. Boukraa, N. Battaglini, and B. Piro, "Graphene-based materials and their applications in electrolyte-gated transistors for sensing," *Synthetic Metals*, vol. 295, May 2023, doi: 10.1016/j.synthmet.2023.117355.
- [2] S.-J. Tsai and R.-J. Yang, "Bimodal behaviour of charge carriers in graphene induced by electric double layer," *Scientific Reports*, vol. 6, no. 1, Jul. 2016, doi: 10.1038/srep30731.
- [3] A. K. Geim, "Graphene: status and prospects," *Science*, vol. 324, no. 5934, pp. 1530–1534, Jun. 2009, doi: 10.1126/science.1158877.
- [4] G. C. Ghivela and J. Sengupta, "The promise of graphene: A survey of microwave devices based on graphene," *IEEE Microwave Magazine*, vol. 21, no. 2, pp. 48–65, Feb. 2020, doi: 10.1109/MMM.2019.2951967.
- [5] G. C. Ghivela and J. Sengupta, "Modeling and computation of double drift region transit time diode performance based on graphene-SiC," *International Journal of Numerical Modelling: Electronic Networks, Devices and Fields*, vol. 32, no. 5, 2019, doi: 10.1002/jnm.2601.
- [6] G. Zhao *et al.*, "The physics and chemistry of graphene-on-surfaces," *Chemical Society Reviews*, vol. 46, no. 15, pp. 4417–4449, 2017, doi: 10.1039/C7CS00256D.
- [7] G. H. Nayana and P. Vimala, "Monolayer and bilayer graphene field effect transistor using Verilog-A," *International Journal of Reconfigurable and Embedded Systems (IJRES)*, vol. 10, no. 1, pp. 56–64, Mar. 2021, doi: 10.11591/ijres.v10.i1.pp56-64.
- [8] H. M. Marhoon and N. Qasem, "Simulation and optimization of tuneable microstrip patch antenna for fifth-generation applications based on graphene," *International Journal of Electrical and Computer Engineering (IJECE)*, vol. 10, no. 5, pp. 5546–5558, Oct. 2020, doi: 10.11591/ijece.v10i5.pp5546-5558.
- [9] R. Al-Mudhafer and H. A. Jawad, "Plasmonic hybrid terahertz photomixer of graphene nanoantenna and nanowires," *International Journal of Electrical and Computer Engineering (IJECE)*, vol. 12, no. 3, pp. 2711–2720, Jun. 2022, doi: 10.11591/ijece.v12i3.pp2711-2720.
- [10] A. Acharyya, "1.0–10.0 THz radiation from graphene nanoribbon based avalanche transit time sources," *physica status solidi (a)*, vol. 216, no. 7, Apr. 2019, doi: 10.1002/pssa.201800730.
- [11] G. C. Ghivela and J. Sengupta, "Numerical study of magnetic field effect on graphene based IMPATT source," *Superlattices and Microstructures*, vol. 137, Jan. 2020, doi: 10.1016/j.spmi.2019.106365.
- [12] G. C. Ghivela and J. Sengupta, "Space charge studies in graphene based avalanche transit time devices," *Superlattices and Microstructures*, vol. 155, Jul. 2021, doi: 10.1016/j.spmi.2021.106899.

- [13] G. C. Ghivela, "Prospects of graphene-based heat sink and its computational thermal analysis in avalanche transit time devices," *Journal of Computational Electronics*, vol. 22, no. 4, pp. 982–989, Aug. 2023, doi: 10.1007/s10825-023-02047-3.
- [14] J. Pradhan, S. R. Pattanaik, S. K. Swain, and G. N. Dash, "Low noise wide bandgap SiC based IMPATT diodes at sub-millimeter wave frequencies and at high temperature," *Journal of Semiconductors*, vol. 35, no. 3, Mar. 2014, doi: 10.1088/1674-4926/35/3/034006.
- [15] G. C. Ghivela, J. Sengupta, and M. Mitra, "Ka band noise comparison for Si, Ge, GaAs, InP, WzGaN, 4H-SiC-based IMPATT diode," *International Journal of Electronics Letters*, vol. 7, no. 1, pp. 107–116, Jan. 2019, doi: 10.1080/21681724.2018.1460869.
- [16] J. Pradhan and S. R. Pattanaik, "IMPATT diodes based on GaAs for millimeter wave applications with reference to Si," in *Post-Transition Metals*, IntechOpen, 2021.
- [17] S. M. Sze and R. M. Ryder, "Microwave avalanche diodes," *Proceedings of the IEEE*, vol. 59, no. 8, pp. 1140–1154, 1971, doi: 10.1109/PROC.1971.8360.
- [18] H. J. Shin *et al.*, "Unsaturated drift velocity of monolayer graphene," *Nano Letters*, vol. 18, no. 3, pp. 1575–1581, Mar. 2018, doi: 10.1021/acs.nanolett.7b03566.
- [19] M. Ghadiry, A. B. A. Manaf, M. Nadi, M. Rahmani, and M. T. Ahmadi, "Ionization coefficient of monolayer graphene nanoribbon," *Microelectronics Reliability*, vol. 52, no. 7, pp. 1396–1400, Jul. 2012, doi: 10.1016/j.microrel.2012.02.017.
- [20] M. Orlita *et al.*, "Approaching the dirac point in high-mobility multilayer epitaxial graphene," *Physical Review Letters*, vol. 101, no. 26, Dec. 2008, doi: 10.1103/PhysRevLett.101.267601.
- [21] A. Acharyya, "Impact ionization rate of electrons in bilayer graphene nanoribbons," *Journal of Electronic Materials*, vol. 48, no. 11, pp. 7169–7176, Nov. 2019, doi: 10.1007/s11664-019-07528-5.
- [22] A. Kundu and M. Mukherjee, "Physics based non-linear large-signal analysis of multiple-graphene layer exotic pin (p++-n--n++) devices and ultra-fast SPST/SPDT/SPMT switches on Si/3C-SiC (100) substrates for application in THz-communication," *Microsystem Technologies*, vol. 28, no. 3, pp. 683–704, Mar. 2022, doi: 10.1007/s00542-019-04325-2.
- [23] Y. Yin, Z. Cheng, L. Wang, K. Jin, and W. Wang, "Graphene, a material for high temperature devices-intrinsic carrier density, carrier drift velocity and lattice energy," *Scientific Reports*, vol. 4, no. 1, Jul. 2014, doi: 10.1038/srep05758.
- [24] A. Di Bartolomeo, "Graphene Schottky diodes: An experimental review of the rectifying graphene/semiconductor heterojunction," *Physics Reports*, vol. 606, pp. 1–58, Jan. 2016, doi: 10.1016/j.physrep.2015.10.003.
- [25] M. G. Ancona, "Electron transport in graphene from a diffusion-drift perspective," *IEEE Transactions on Electron Devices*, vol. 57, no. 3, pp. 681–689, Mar. 2010, doi: 10.1109/TED.2009.2038644.
- [26] H. K. Gummel and J. L. Blue, "A small-signal theory of avalanche noise in IMPATT diodes," *IEEE Transactions on Electron Devices*, vol. 14, no. 9, pp. 569–580, Sep. 1967, doi: 10.1109/T-ED.1967.16005.
- [27] A. Acharyya *et al.*, "Large-signal characterization of DDR silicon IMPATTs operating up to 0.5 THz," *International Journal of Microwave and Wireless Technologies*, vol. 5, no. 5, pp. 567–578, Oct. 2013, doi: 10.1017/S1759078713000597.
- [28] A. Acharyya *et al.*, "IMPATT devices based on group III-V compound semiconductors: prospects as potential terahertz radiators," *HKIE Transactions*, vol. 21, no. 3, pp. 135–147, Jul. 2014, doi: 10.1080/1023697X.2014.945231.
- [29] A. Acharyya, "Gallium phosphide IMPATT sources for millimeter-wave applications," *Iranian Journal of Electrical and Electronic Engineering*, vol. 14, no. 2, pp. 143–152, 2018.

## BIOGRAPHIES OF AUTHORS



**Mamata Rani Swain** received the Engineer Degree in Electronics and Telecommunication Engineering from Bhadrak Institute of Technology in 2003. She received the master degree in Telecommunication Engineering from Biju Patnaik University of Technology (BPUT), Odisha, India in 2010. Currently she is working as assistant professor, Department of Electronics and Telecommunication Engineering in Synergy Institute of Technology, Bhubaneswar, Odisha, India. Her research interests are impact ionization avalanche transit time (IMPATT) diode and 2-D materials. She can be contacted at email: swain.mamata201@gmail.com.



**Pravash Ranjan Tripathy** received master degree in Electronics from Sambalpur University in the year 2001 and did his Ph.D. in Electronics from Sambalpur University in the year 2011. He is working as Dean Academics at Gandhi Engineering College Bhubaneswar. He has more than 22 years of teaching and research experience. He was associate professor and head in Department of Electronics and Communication Engineering at Hi-Tech College of Engineering Bhubaneswar and Purushottam Institute of Engineering and Technology Rourkela. He is known for his work on microwave devices and particular on IMPATT devices for RF Communication. Beside this he has other areas of research like wide band gap semiconductor material and devices for power electronics application. He can be contacted at email: pravashrt76@yahoo.co.in.